Oxyacetylene torch testing and microstructural characterization of tantalum carbide

Paul, A.; Binner, JGP; Vaidhyanathan, B.; Heaton, A. C J; Brown, P. M.

DOI:
10.1111/jmi.12028

Oxyacetylene Torch Testing and Microstructural Characterisation of Tantalum Carbide

A. Paul[a], J.G.P. Binner[a], B. Vaidhyanathan[a], A.C.J. Heaton[b] and P.M. Brown[b]

[a]Department of Materials, Loughborough University, UK, LE11 3TU

[b]DSTL, Porton Down, Salisbury, UK, SP4 0JQ

Abstract

Tantalum carbide samples have been subjected to high temperature testing at ~2300°C using an oxyacetylene torch to evaluate their potential for ultra-high temperature applications. Whilst large samples cracked during the rapid heating, indicating their inability to withstand thermal shock, small samples survived the severe test conditions. The oxidation products formed were characterised and found to comprise different phases of Ta_2O_5. The ultra-high temperature experienced by the samples resulted in the formation of many interesting microstructures, including the formation of submicron sized grains, which has not been reported previously in the literature, as well as the expected evidence of melting.

Keywords: tantalum carbide, ultra-high temperature, oxyacetylene

Introduction

Tantalum carbide, TaC, is a refractory carbide with one of the highest known melting points (3985°C) and is considered as an ultra-high temperature ceramic, UHTC (Andersson *et al*., 2000,Tulhoff., 2000). There are several subcarbides of the Ta-C system with lower carbon contents, however, the monocarbide, TaC, is the most widely used phase. Its main application is in cemented carbide as its addition improves the high temperature fatigue strength, thermal shock resistance, hot hardness and resistance against cratering and oxidation (Andersson *et al*., 2000,Tulhoff., 2000). TaC is a potential candidate for ultra high temperature applications such as leading edges and nose caps for hypersonic vehicles, rocket thrusters, combustor linings, etc., because of its high melting point.

There are only limited studies on the high temperature oxidation behaviour of TaC materials. Desmaison-Brut et al. (Desmaison-Brut *et al*., 1997) compared the oxidation behaviour of hot isostatically pressed TaC and Ta_2C under isothermal and isobaric conditions in a dynamic flow of pure oxygen using a microbalance at relatively low temperatures of up to 850°C. They reported superior oxidation resistance for Ta_2C and the formation of an oxycarbide layer at the Ta_2C-Ta_2O_5 interface, whereas no such oxycarbide was observed for TaC. Thermogravimetric analysis, at temperatures up to 1500°C, has been used to compare the oxidation behaviour of TaC, TaC+10 wt% TaB_2 and pure TaB_2 (Zhang *et al*., 2008). It was observed that the oxidation resistance of TaC was marginally improved by the addition of TaB_2. Sciti et al. (Sciti *et al*., 2009) studied the oxidation of TaC with separate additions of 15 vol% of

$MoSi_2$ and $TaSi_2$ at 1600°C in static air, exposing the samples for 15 min. Both materials were found to undergo severe oxidation, which considerably reduced the strength of the composites.

There are no reports on the ultra-high temperature testing of TaC ceramics using an oxyacetylene flame and the resulting morphology of the microstructure. The present paper compares the oxidation behaviour and microstructure at and around the ablation centre of TaC samples subjected to oxyacetylene torch testing at temperatures up to ~2300°C.

Experimental

100 x 100 x 10 mm TaC blocks were obtained from Cerac Inc., Milwaukee, USA. According to the manufacturer, the sample was densified via hot pressing and had a purity of 99.5%. The density of the sample was measured using the Archimedes principle in water and was found to be 93% of theoretical. 15 and 32 mm diameter discs for oxyacetylene torch testing were machined out of the ceramic block using electrical discharge machining (EDM).

A purpose built oxyacetylene torch test rig was used to perform the high temperature oxidation testing. A schematic of the torch test facility is shown in Figure 1. Oxygen and acetylene in a 1.35:1 ratio was fed through a welding nozzle (No.13 nozzle, BOC Industrial, Surrey, UK) to produce an oxidising flame. For testing, the samples were positioned in a water cooled graphite holder that was then manually moved slowly into the hot zone of the flame.

The samples were held there for 60 seconds and then the flame was extinguished allowing the samples to cool down naturally. During the test, the temperature distribution was recorded using a modified infrared thermal imaging camera (Thermovision A40, FLIR Systems AB, Danderyd, Sweden) and the peak temperature was recorded using a Marathon MR1SCSF two-colour infrared pyrometer (Raytek GmbH, Berlin, Germany). The back face temperature of the samples was also recorded during testing using a K-type thermocouple connected to a data logger.

For testing the 15 mm diameter discs, the samples were placed in a carbon-carbon insert prior to fixing inside the graphite sample holder whereas the 32 mm samples were fixed directly within the holder. For the 15 mm diameter discs, distances of 10, 15 and 20 mm were used between the sample and the nozzle to alter the peak temperature and heating profile. Four 32 mm diameter samples were also tested at 10 mm distance, but three of them shattered within a few seconds of moving into the flame, even before reaching the peak temperature.

The surface microstructure of the TaC before and after oxyacetylene torch testing was characterised using a field emission gun scanning electron microscope (FEGSEM, LEO 1530VP, Carl Zeiss SMT, Oberkochen, Germany) and the chemical composition was examined using energy dispersive spectroscopy, EDS (EDAX, EDAX Inc., NJ, U.S.A.). The microstructure and composition beneath the oxide layer was also analysed after removing the oxide; the adhesion between the base layer and oxide was

poor and the latter was easily removed. X-ray diffraction patterns of the as-received TaC and the various oxidation products formed after the oxyacetylene torch tests were recorded with a Bruker D8 model diffractometer (Bruker AXS GmbH, Karlsruhe, Germany) using Cu-Kα radiation. The samples were cross sectioned after the oxyacetylene test, polished and characterised using FEGSEM and EDS.

Results

The microstructure, EDS spectrum and XRD of the TaC before the oxyacetylene torch test is shown in Figure 2. It can be seen that the grain size distribution is unimodal with an average size of 2-3 μm. Porosity is clearly visible as the ceramic was only 93% dense. From the XRD pattern it can be seen that all the peaks correspond to the face centred cubic structure.

The time temperature profiles for the 15 mm diameter discs held at different distances from the nozzle during torch testing are given in Figure 3. It can be seen that increasing distance between the sample and nozzle resulted in much lower heating rates and peak front face temperature, as expected. The heating rate for the first 5 seconds decreased from 330°C s^{-1} to 325°C s^{-1} to 275°C s^{-1}, whereas the peak front face temperature decreased from 2300°C to 2190°C and then to 1990°C as the distance increased from 10 mm to 15 mm and then to 20 mm respectively. It is well known that the gas flow rate and gas flow ratio has a pronounced influence on the nature of the flame and its temperature; these two parameters were kept constant and only the distance was varied. The oxyacetylene flame has an inner cone and an outer

feather and the peak temperature is at the tip of the inner cone (Campbell., 1919). Figure 4 shows a view of one of the samples at 15 mm from the tip of the nozzle, through a welding goggle, during testing. It can be seen that the inner cone of the flame is just touching the sample surface. The length of this cone was determined to be ~16 mm so this sample was exposed to the highest temperature. As well as a decrease in temperature, a decrease in gas flow velocity was also expected with an increase in distance between the sample and the nozzle tip, though the magnitude of this could not be quantified.

Images of the samples after testing are shown in Figure 5. The front faces can be seen to be covered with a white layer indicating that the expected oxidation had occurred. The surface oxide layer completely detached from the base material for the sample tested at 20 mm from the nozzle tip, whereas there was some adhesion for the other samples, possibly due the formation of liquid phases at the test temperature and their subsequent solidification on cooling. However, no signs of surface erosion or cracking were observed for the 20 mm sample, whilst erosion, melting and cracking were all observed for the other two distances. On cross sectional examination, the cracks were found to propagate into the bulk.

The response of the 32 mm diameter TaC discs to the flame was completely different due to the large thermal gradients that developed. Unlike the 15 mm diameter discs, which were embedded in a carbon-carbon holder, these samples were held directly by the graphite sample holder using three graphite

bolts. During the test, there was rapid heating and severe thermal gradients. As the samples tried to expand, the graphite bolts resulted in stresses being generated that resulted in crack formation. Three out of four 32 mm TaC discs tested shattered and fell out of the sample holder before reaching even 1000°C. Whilst the fourth sample cracked, it didn't fall out allowing the 60 second test to be completed, Figure 6. The cracks originated from the centre of the sample, where the oxyacetylene flame was focused, and propagated to the points where it was held by the bolts; highlighted by the arrows. One way to avoid this cracking in the future is to eliminate any stresses from the sample holder. The thermal gradients on the 32 mm disc are shown in Figure 7 and the peak back face temperature was recorded to be ~1050°C.

The formation of a white layer was also observed on the 32 mm diameter sample front surface, together with straw coloured, frozen liquid phases with a clear melt boundary. X-ray diffraction patterns of both the white surface layer and the solidified molten structure are shown in Figure 8 (a) and (b); the layer comprised α and β phases of Ta_2O_5, with the strongest peak corresponding to that of the α. Similarly, the frozen droplets were also found to comprise mainly α, with small amounts of β also being detected.

Cross sectional analysis of the 15 mm discs was performed to compare the thickness of the oxide layers formed and the chemical compositions, Figure 9. An increase in oxide layer thickness was expected with an increase in temperature, but a decrease was actually observed at the highest temperatures due to the melting of the Ta_2O_5 and its removal by the gas flow.

This clearly highlights the disadvantage of using this type of material at ultra-high temperatures when a high velocity gas flow is present. EDS analysis of the frozen droplets and the oxide layer indicated the presence of Ta and O, whereas the bulk, unaffected material continued to reveal only Ta and C.

The surface of the disc after oxyacetylene torch testing can be divided into three separate zones, each with a different morphology, Figure 6. Zone 1 is at the flame tip, where the flame directly impinged the sample and hence the temperature was highest. Zone 2 is the flow zone; the temperature experienced was lower and the molten products formed in zone 1 were swept across by the high velocity gas flow from the torch nozzle. Zone 3 experienced the lowest temperature and no melting was observed. A clear melt boundary is visible between zones 2 and 3.

The detailed microstructural analysis of the sample after testing revealed several interesting features. The white oxide layer formed on the surface of the sample in zone 1 was found to be highly porous, Figure 10 (a). This is believed to be due to the escape of the CO/CO_2 gases formed at high temperatures and the porosity allows easy diffusion of oxygen towards the bulk of the sample. The microstructure beneath the white oxide layer in zone 1 is shown in Figure 10 (b). This region is not as porous as the surface layer, indicating only a partial oxidation and the individual grains were observed to have small pores within them. EDS analysis of this region detected mainly Ta and O. If the sample was held at the testing temperature for longer, it is

believed that these grains would also have developed porosity similar to that of the surface layer.

Many interesting microstructures were observed in zone 2, the area between the flame tip and the melt boundary. Figure 11 (a) shows the formation of large columnar grains growing in a radial direction. These will have been formed as a result of the high velocity flame pushing the molten oxide out of zone 1. A higher magnification view of these columnar grains indicates the presence of very fine, dense looking grains, Figure 11 (b), (c) and (d). EDS analysis (not shown) detected only Ta and O in these fine grains.

Near to the melt boundary, but within zone 2, the columnar grains were oriented in random directions because of the rapid cooling, as shown in Figure 12. The segregation of a secondary phase was identified on some of the frozen droplets and EDS analysis confirmed the presence of Fe, which is believed to have come from the impurities present in the starting material, Figure 13, although no Fe was detected on the EDS of the starting material, Figure 2 (b). It is assumed that the very low quantities of Fe present in the starting material were uniformly distributed and during ultra-high temperature testing they melted and coalesced in the Ta_2O_5 droplets. A similar type of segregation was reported by Sautereau et al. (Sautereau & Mocellin., 1974) after the thermal etching of sintered TaC and NbC samples at 1400°C. They reported that the impurities present in the starting powders coalesced and formed droplets, predominantly at the grain centres, during the thermal

etching process. The use of Fe as a sintering aid during the hot pressing of TaC has been reported (Scholz., 1963).

Discussion

Oxidation of tantalum carbide has been observed to proceed with the formation of a porous, non-protective oxide scale. Melting of the scale is observed when the test temperature is >1900°C. The major reactions taking place during the oxidation of TaC are given by equations 1 and 2 (Desmaison-Brut *et al*., 1997).

$$4TaC + 7O_2 \rightarrow 2Ta_2O_5 + 4CO \qquad \text{Eqn (1)}$$

$$2TaC + 9/2O_2 \rightarrow Ta_2O_5 + 2CO_2 \qquad \text{Eqn (2)}$$

The formation of other oxides, such as TaO_2 and Ta_2O_3, has also been reported at intermediate temperatures of around 900-1300°C, depending on the oxygen partial pressure (Chen *et al*., 2010). No such oxides were observed after oxyacetylene torch testing, though they might have been formed during the heating stages.

The indexing of the X-ray diffraction pattern of the low temperature form of Ta_2O_5 has always confused crystallographers. Most of the intense diffraction lines can be indexed using an orthorhombic unit cell; however, many of the weak lines have not been interpreted unambiguously. The reason for this is that the position of the weak lines is dependent on the nature of the heat treatment and the amount of cation and anion impurities (Roth *et al*., 1970). The situation is made more complex in the present study because of the rapid

heating and cooling involved. It has also been reported that the high temperature polymorph (α-Ta_2O_5) undergoes several phase transformations on quenching. Although it is triclinic at room temperature, it is monoclinic at intermediate temperatures and tetragonal at the temperature at which it is stable (Waring & Roth., 1968). XRD patterns of the oxide layers from the current study indicated the presence of both α and β-Ta_2O_5. The crystal structure of the α-phase was observed to be triclinic. β-Ta_2O_5 is a low temperature phase with a transition temperature of 1320±20°C to the α phase, which is stable at high temperature (Lagergren & Magnéli., 1952). Reisman et al., (Reisman *et al*., 1956) reported a slightly higher transformation temperature of 1360±5°C after heating Ta_2O_5 using an oxy-gas flame and also suggested that this transformation is sluggish but completely reversible. Quenching of the molten phases resulted in a straw coloured, crystalline Ta_2O_5 that had a similar structure to the frozen droplets from the current study. For Reisman et al. (Reisman *et al*., 1956) however, their X-ray diffraction pattern of the solidified structure revealed the presence of just the α-phase whereas β-phase was also observed in the present study. The presence of the latter is expected to be due to the rapid heating and cooling and the sluggish transformation behaviour. An increase in the α-phase intensity for the frozen droplets is possibly due to the higher temperature experienced by the droplets and the minimal time available for this phase to revert to β due to rapid cooling. The presence of ε and δ-phases (Izumi & Kodama., 1979), and many high pressure phases, (Filonenko & Zibrov., 2001,Zibrov *et al*., 2000) are also reported in the literature, but none of them was observed in the present work. Even though the melting point of TaC is

around 3985°C, it is reported to undergo oxidation at temperatures as low as 800°C (Zhang *et al*., 2008) and the resulting oxides melt at around 1800°C (1785±30°C for β-Ta_2O_5 and 1872°C for α-Ta_2O_5 (Reisman *et al*., 1956)), which is well below the oxyacetylene torch test temperatures used in the present study.

The XRD results are not completely in agreement with those reported after the oxidation of C-TaC-C composites at temperatures up to 1400°C (Chen *et al*., 2010), where the formation of a hexagonal structure (δ-Ta_2O_5) was reported at temperatures below 900°C. This then transformed to an orthorhombic (β-Ta_2O_5) structure above this temperature. This difference could be due to the large difference in testing temperatures and the more oxidising conditions.

Gaseous CO/CO_2 is produced as a by-product during the oxidation of TaC. The escape of these gases produces continuous porosity in the oxide layer, as reported by Courtright et al.(Courtright *et al*., 1991). The pores act as pathways for both the inward transport of oxygen and further outward diffusion of CO, preventing CO build up and catastrophic delamination of the oxide layer under static oxidation conditions. The delamination of the oxide layer observed in the current study was again partially due to the rapid heating rates involved, these will have limited the time available for the gasses formed to escape. Further factors are outlined below.

The pores present in the grains beneath the fully oxidised surface layer will have been created by the partial internal oxidation of the TaC grains. Similar observations were made by Courtright et al.(Courtright *et al*., 1991). A well-defined carbide-oxide boundary layer indicated the reaction front. The oxidation reaction taking place at this interface can be assumed to control the rate of oxidation. Similar interfacial oxidation reactions were also reported for other high temperature carbides such as HfC and ZrC with an oxygen gradient from the oxide layer to the carbide. The diffusion of oxygen into the carbide limits the rate of the reaction (Shimada., 2001). A change in the rate controlling mechanism at ~1800°C has also been reported in the literature. The lower temperature kinetics can be explained by assuming that oxide growth is controlled by O_2, CO and CO_2 gaseous transport through the interconnected pores in the oxide. This process became less important at increasing temperatures as the oxide sintered and the effective volume available for gaseous diffusion was reduced (Courtright *et al*., 1991). During the oxyacetylene torch testing, the oxides formed melted making it more difficult for the O_2 to diffuse through the viscous liquid phase compared to diffusing through the interconnected porous oxide. Also, near the tip of the flame, the melt formed was pushed away from the flame front by the high velocity gas flow hitting the sample, exposing fresh surfaces for oxidation and influencing the rate of the reaction. The formation and escape of any intermediate oxides such as TaO_2 and Ta_2O_3 will also have led to the generation of more porosity, helping the rapid inward diffusion of oxygen and accelerating the oxidation process (Chen *et al*., 2010). In addition to gas build up, the difference in coefficient of thermal expansion between the oxide and

the underlying carbide can also play a role in delamination. The CTE of Ta_2O_5 is reported to be around 2.9 x 10^{-6}/°C from room temperature to 500°C(Moldovan *et al*., 2004) whereas that of TaC is 6.29 x 10^{-6}/°C at room temperature(Tulhoff., 2000).

The molten oxides recrystallised on cooling forming columnar grains. The formation of the submicron grains is expected to be due to the formation of tantalum suboxides, including TaO_2 and Ta_2O_3 at intermediate temperature of oxidation, probably during the heating up stage. The formation temperature of some of these suboxides are reported to be <600°C (Chang & Phillips., 1969). It is believed that some of these oxides will have vaporised at the ultra-high temperatures being used (Chen *et al*., 2010) and then deposited at regions of relatively lower temperature on the sample surface. They would subsequently undergo sintering, leading to the formation of dense-looking submicron grains on the surface. The presence of molten phases is expected to act as nucleation sites for the growth of these grains.

Conclusions

Even though TaC has the highest melting point amongst all the potential materials for UHTC applications, the results of the oxyacetylene torch testing proved its inability to fulfil the requirements for such applications. TaC was unable to withstand the high thermal shocks experienced during the test, leading to severe cracking. It oxidised at temperatures well below the melting point of the carbide and the oxides melted at temperatures below 1900°C

rendering these materials unsuitable for applications requiring ultra-high temperature (>2000^{o}C) resistance. Moreover, the oxide layer formed was porous and not completely adherent, offering little or no additional protection at elevated temperatures. The oxides were found to comprise the low and high temperature stable phases of Ta_2O_5. The formation of submicron grains was expected to be due to the volatilisation, deposition and subsequent sintering of the oxide phases formed at intermediate temperatures.

Acknowledgements

The authors thank the UK's Defence Science and Technology Laboratory (DSTL) for providing the financial support for this work under contract number DSTLX-1000015267 as well as the US Air Force Research Laboratory's Materials and Manufacturing Directorate for on-going collaborations.

References

Andersson K., Reichert K. & Wolf R. (2000) Tantalum and tantalum compounds. Ullmann's Encyclopedia of Industrial Chemistry, pp. 1-15. Wiley-VCH Verlag GmbH & Co. KGaA.

Campbell L. (1919) Chapter II: Operation. Oxy-Acetylene Welding Manual, pp. 27-38. John Wiley and Sons, Inc., New York.

Chang L.L.Y. & Phillips B. (1969) Phase relations in refractory metal-oxygen systems. J. Am. Ceram. Soc. 52, 527-533.

Chen Z., Xiong X., Li G. & Wang Y. (2010) Mechanical properties and oxidation behaviors of carbon/carbon composites with C-TaC-C multi-interlayer. J. Mater. Sci. 45, 3477-3482.

Courtright E.L., Prater J.T., Holcomb G.R., Pierre G.R.S. & Rapp R.A. (1991) Oxidation of hafnium carbide and hafnium carbide with additions of tantalum and praseodymium. Oxid. Met. 36, 423-437.

Desmaison-Brut M., Alexandre N. & Desmaison J. (1997) Comparison of the oxidation behaviour of two dense hot isostatically pressed tantalum carbide (TaC and Ta_2C) materials. J. Eur. Ceram. Soc. 17, 1325-1334.

Filonenko V.P. & Zibrov I.P. (2001) High-pressure phase transitions of M_2O_5 (M = V, Nb, Ta) and thermal stability of new polymorphs. Inorganic Materials 37, 953-959.

Izumi F. & Kodama H. (1979) A new modification of tantalum (V) oxide. Journal of the Less Common Metals 63, 305-307.

Lagergren S. & Magnéli A. (1952) On the tantalum - oxygen system. Acta. Chem. Scand. 6, 444-446.

Moldovan M., Weyant C., Johnson D. & Faber K. (2004) Tantalum oxide coatings as candidate environmental barriers. J. Therm. Spray Technol. 13, 51-56.

Reisman A., Holtzberg F., Berkenblit M. & Berry M. (1956) Reactions of the group VB Pentoxides with alkali oxides and carbonates. III. Thermal and X-ray Phase diagrams of the system K_2O or K_2CO_3 with Ta_2O_5. J. Am. Chem. Soc. 78, 4514-4520.

Roth R.S., Waring J.L. & Parker H.S. (1970) Effect of oxide additions on the polymorphism of tantalum pentoxide. IV. The system Ta_2O_5-Ta_2WO_8. J. Solid State Chem. 2, 445-461.

Sautereau J. & Mocellin A. (1974) Sintering behaviour of ultrafine NbC and TaC powders. J. Mater. Sci. 9, 761-771.

Scholz S. (1963) Some new aspects of hot pressing of refractories. Special Ceramics 1962, Proceedings of a Symposium Held by the British Ceramic Research Association , 293-307.

Sciti D., Silvestroni L., Guicciardi S., Fabbriche D.D. & Bellosi A. (2009) Processing, mechanical properties and oxidation behavior of TaC and HfC composites containing 15 vol% $TaSi_2$ or $MoSi_2$. J. Mater. Sci. 24, 2056-2065.

Shimada S. (2001) Interfacial reaction on oxidation of carbides with formation of carbon. Solid State Ionics 141-142, 99-104.

Tulhoff H. (2000) Carbides. Ullmann's Encyclopedia of Industrial Chemistry (Anonymous), pp. 555-582. Wiley-VCH Verlag GmbH & Co. KGaA.

Waring J.L. & Roth R.S. (1968) Effect of oxide additions on the polymorphism of tantalum pentoxide (System Ta_2O_5 - TiO_2). J. Res. Nat. Bur. Stand. Sect. A. 72A, 175-186.

Zhang X., Hilmas G.E. & Fahrenholtz W.G. (2008) Densification, mechanical properties, and oxidation resistance of TaC-TaB_2 ceramics. J. Am. Ceram. Soc. 91, 4129-4132.

Zibrov I.P., Filonenko V.P., Sundberg M. & Werner P.-. (2000) Structures and phase transitions of B-Ta_2O_5 and Z-Ta_2O_5: two high-pressure forms of Ta_2O_5. Acta Crystallographica Section B 56, 659-665.

Figure Captions

Figure 1 Oxyacetylene torch test set up. (1) Back face thermocouple, (2) water cooling, (3) sample holder, (4) sample, (5) guide rail, (6) protective insulation, (7) oxyacetylene torch, (8) neutral density filter, (9) thermal imaging camera and (10) two-colour pyrometer.

Figure 2 (a) SEM, (b) EDS and (c) XRD of TaC before torch testing.

Figure 3 Time-temperature profiles of TaC discs subjected to oxyacetylene flame at 10, 15 and 20 mm from the nozzle.

Figure 4 View of sample through a welding goggle during oxyacetylene torch testing; the inner cone of the flame is clearly visible. The sample was 15 mmm from the nozzle tip.

Figure 5 Photographic images of the TaC discs after oxyacetylene torch testing at (a) 20 mm, (b) 15 mm and (c) 10 mm distance from the nozzle tip.

Figure 6 32 mm diameter TaC sample after an oxyacetylene torch test. The graphite sample holder is also seen and the arrows indicate the points where the sample was gripped using the bolts. Inset picture shows the TaC disc before testing. The numbers indicate the three different zones observed after torch testing. (1) flame tip zone, (2) flow zone and (3) low temperature zone.

Figure 7 Thermograph showing the thermal gradients developed during the oxyacetylene torch testing of a 32 mm diameter TaC disc at 10 mm from the nozzle. a) Before cracking, b) immediately after cracking and c) before extinguishing the flame.

Figure 8 X-ray diffraction patterns on the 32 mm diameter sample after oxyacetylene torch testing. (a) White layer formed on the surface and (b) solidified molten structure.

Figure 9 Cross sectional images from directly below the flame tip from the 15 mm diameter samples subjected to oxyacetylene torch testing at three different distances from the nozzle, (a) 20 mm (b) 15 mm and (c) 10 mm. The EDS patterns in (d) were recorded from locations 1, 2 and 3 in figure 9 b.

Figure 10 FEGSEM image of (a) white surface oxide layer, (b) partially oxidised grains below the surface layer, (c) the EDS pattern taken on the partially oxidised grains in (b).

Figure 11 (a) SEM image showing the formation of columnar grains. (b) Higher magnification view of the area highlighted by the rectangle in (a). (c) and (d) are higher magnification images of the submicron grains.

Figure 12 SEM images showing the random orientation of grains at the melt boundary.

Figure 13 FEGSEM image showing the formation of a secondary phase on the solidified droplets. EDS detected the presence of Fe along with Ta, O and C.

Figure 1

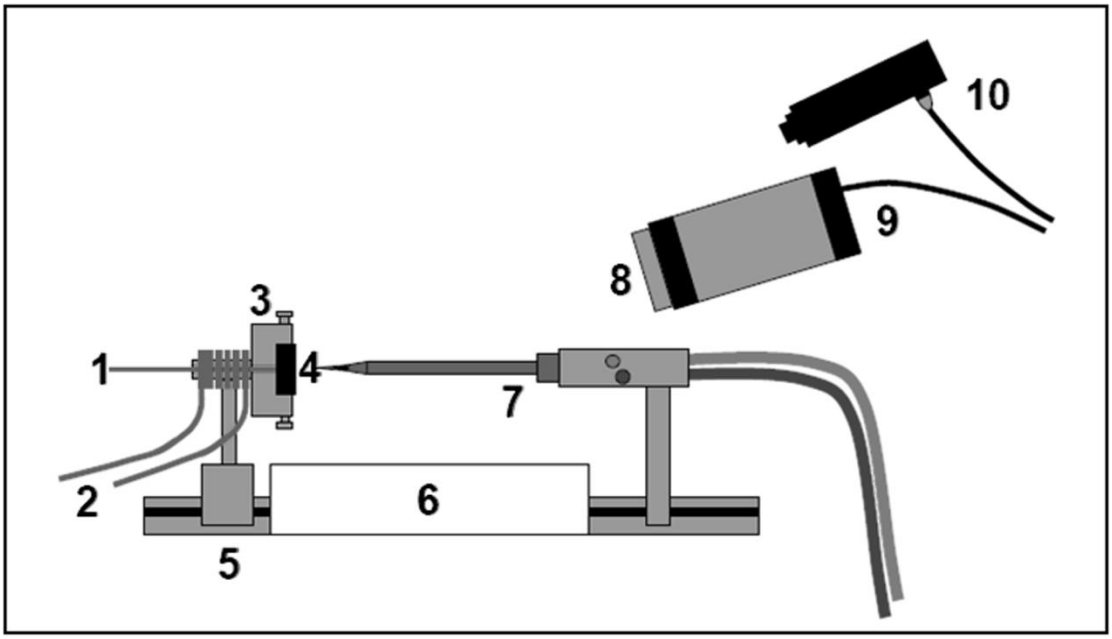

Figure 2

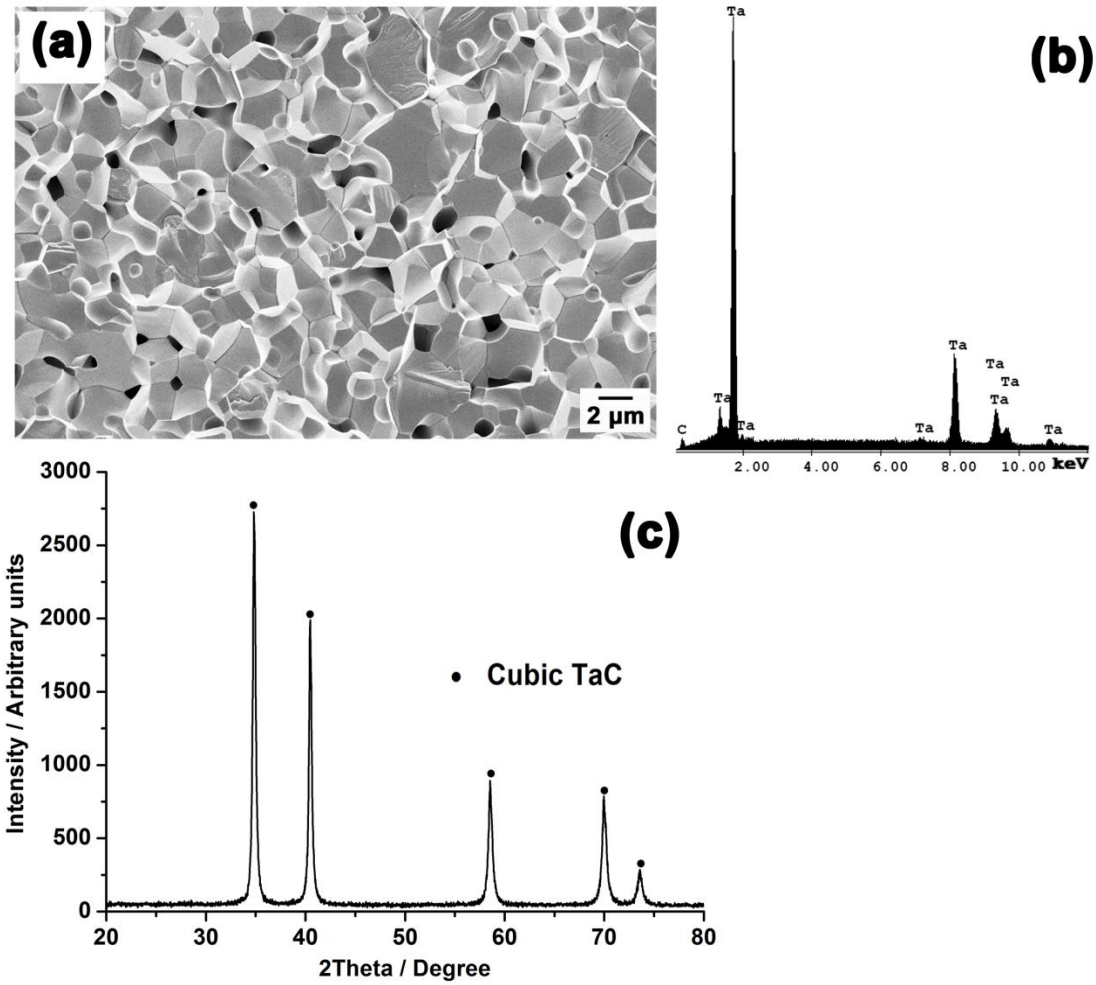

Figure 3

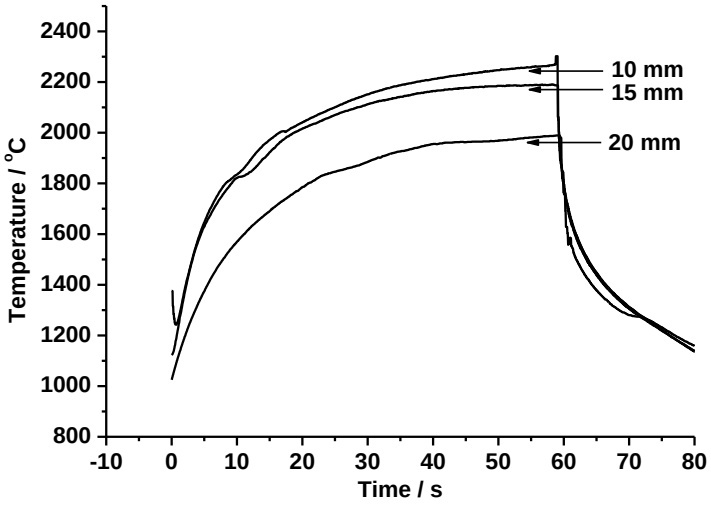

Figure 4

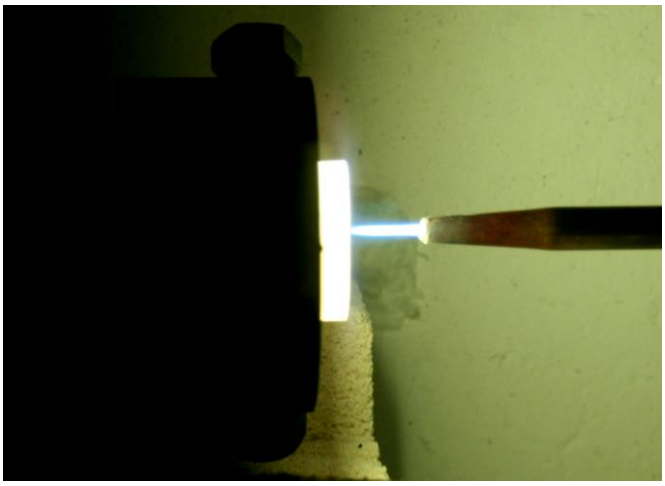

Figure 5

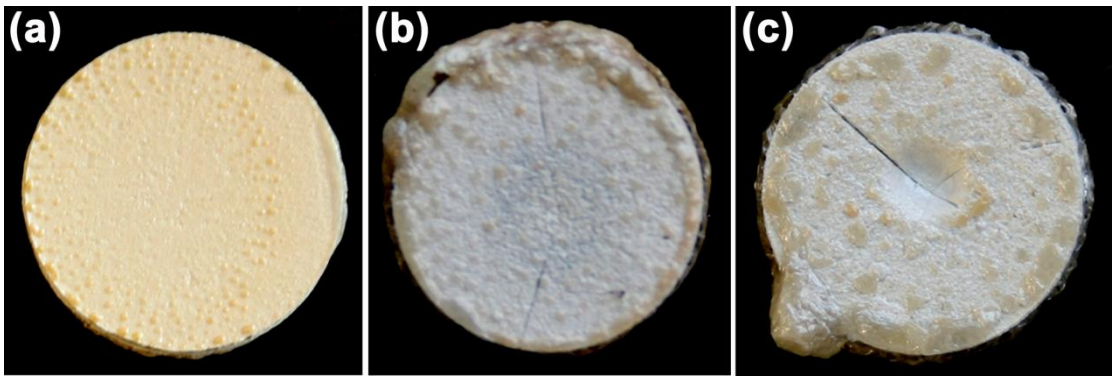

Figure 6

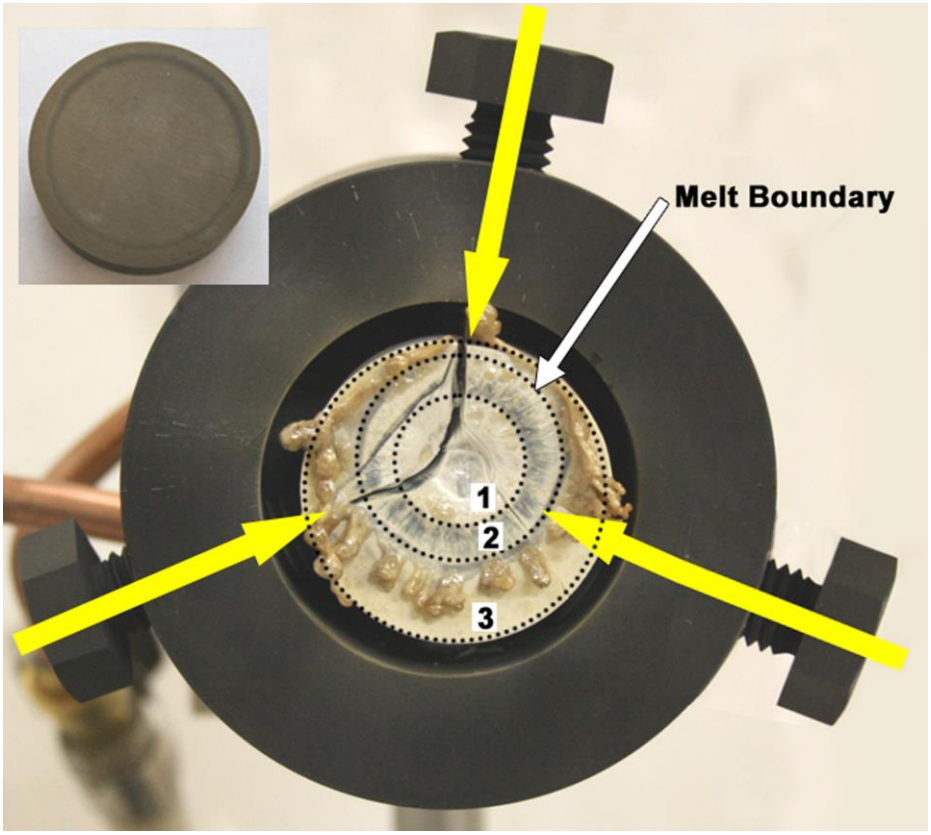

Figure 7

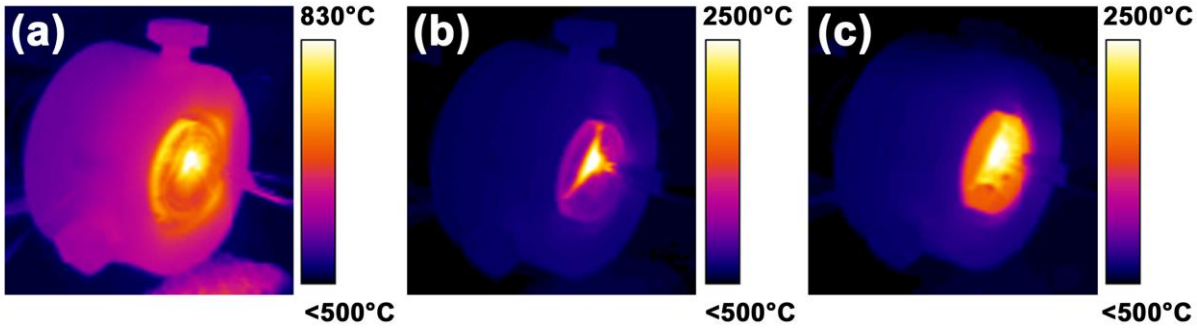

Figure 8

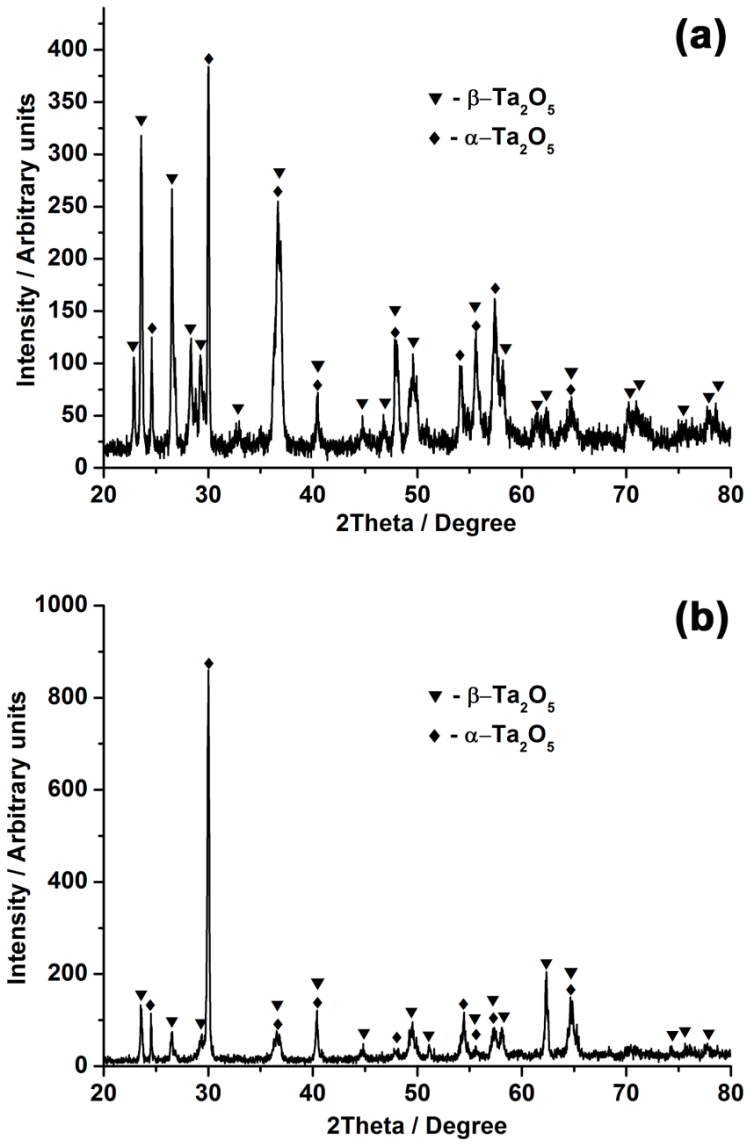
(a)
▼ - β–Ta2O5
♦ - α–Ta2O5
Intensity / Arbitrary units
2Theta / Degree
(b)
▼ - β–Ta2O5
♦ - α–Ta2O5
Intensity / Arbitrary units
2Theta / Degree

Figure 9

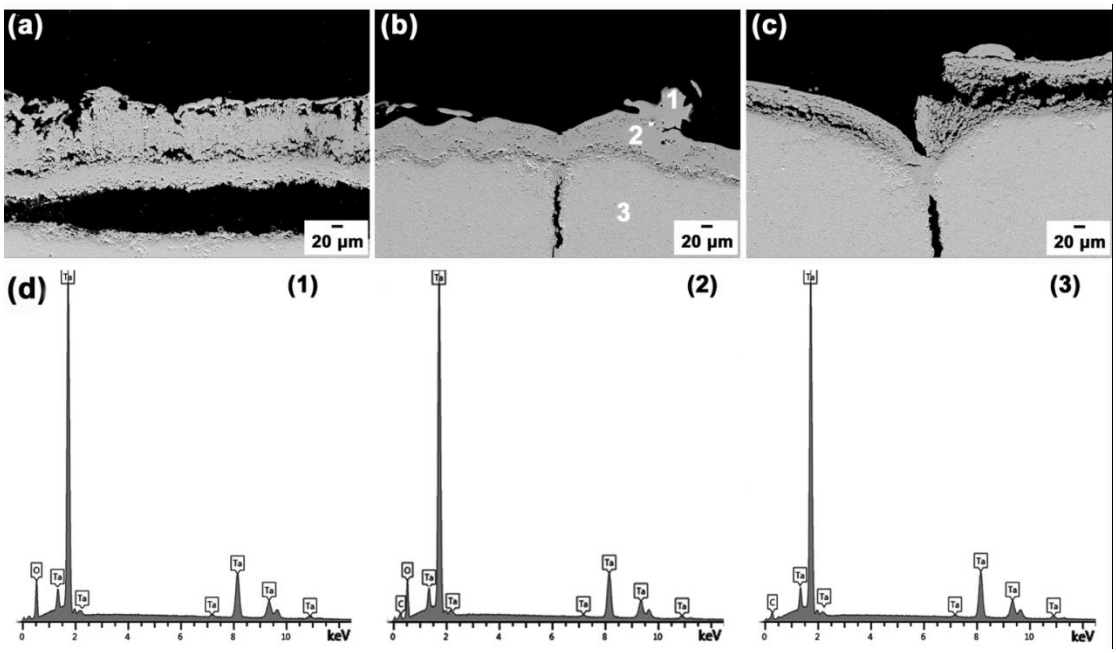

Figure 10

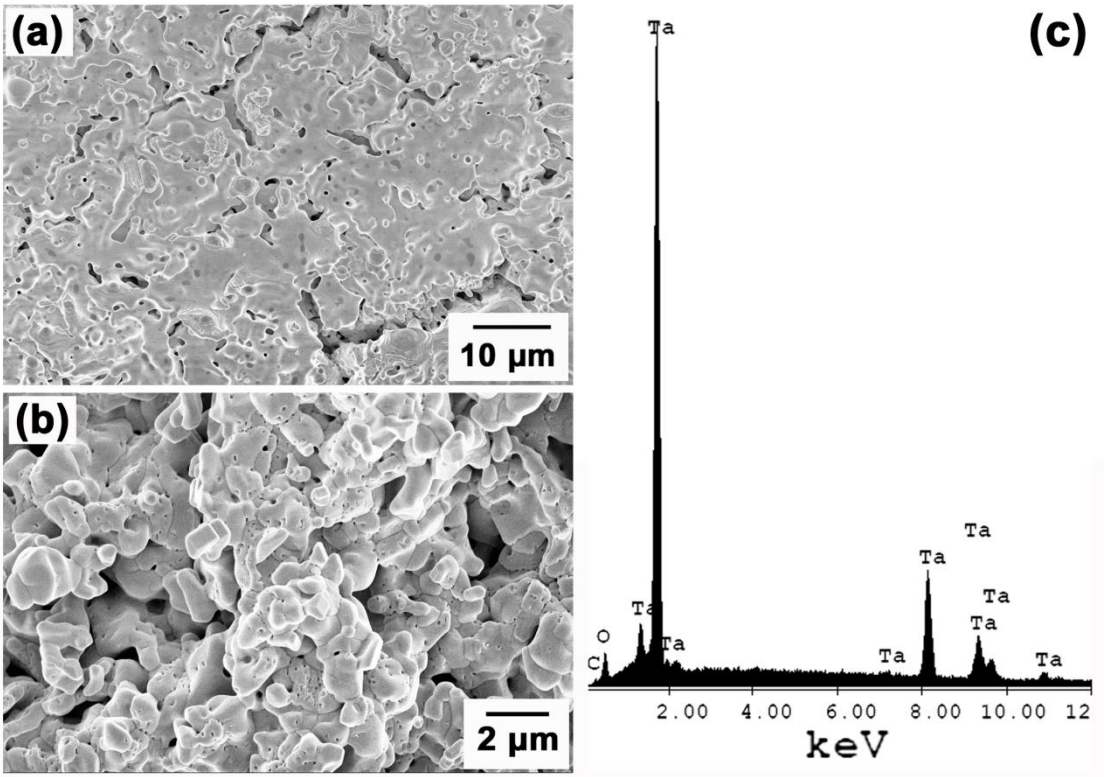

Figure 11

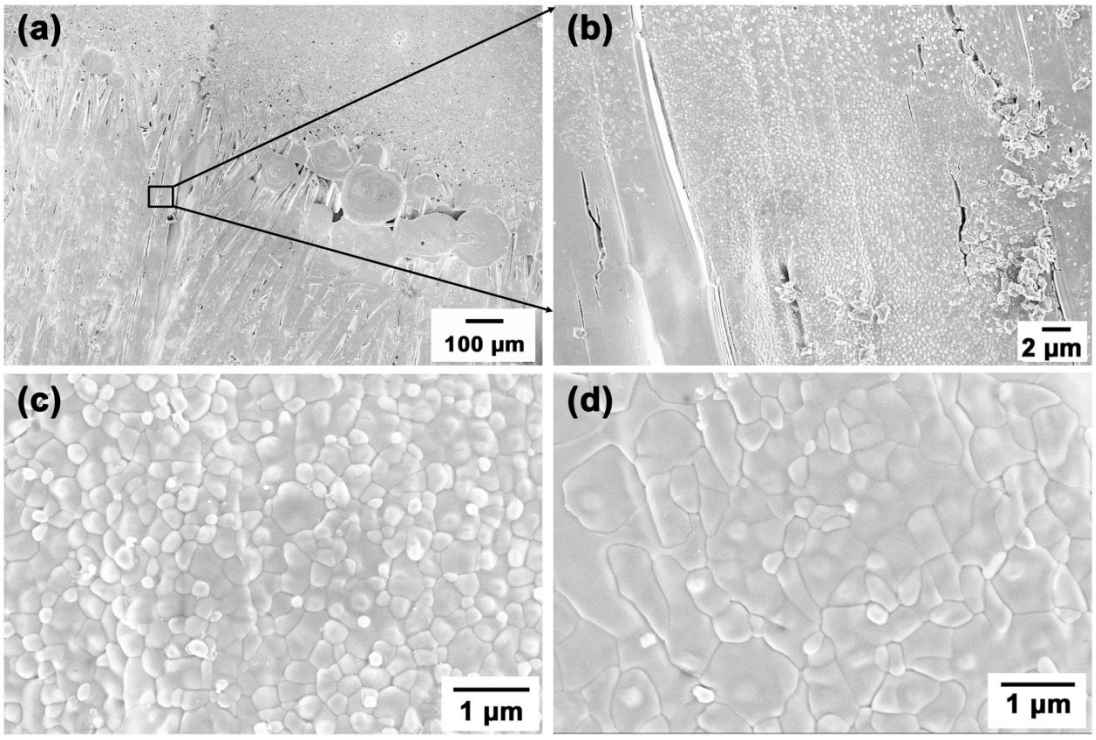

Figure 12

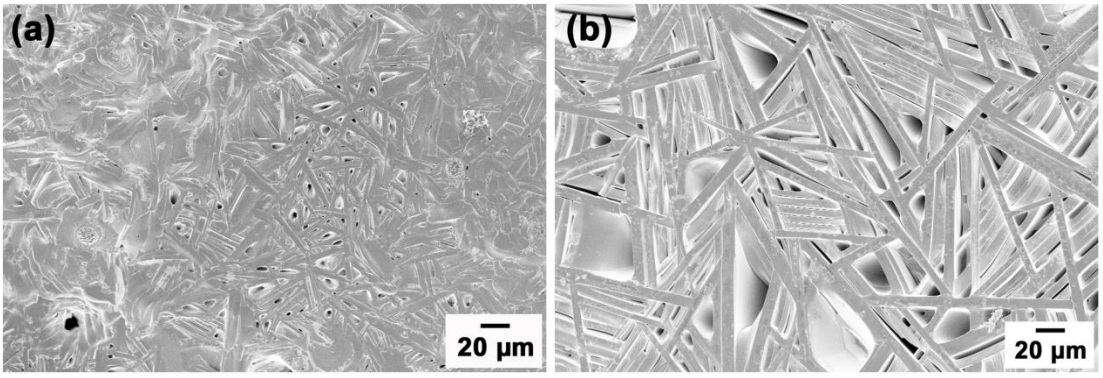

Figure 13

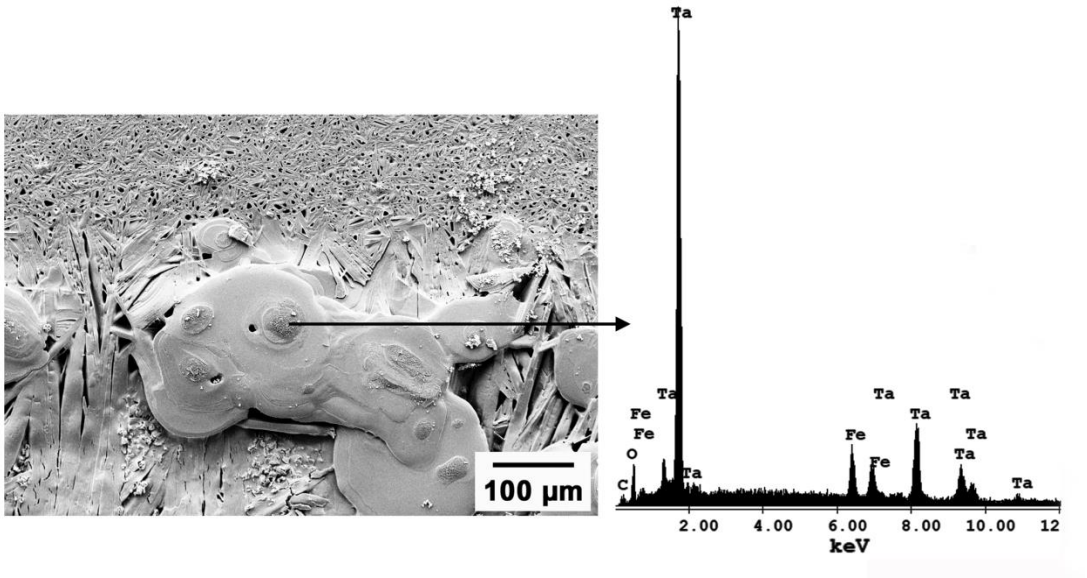
100 µm
Ta
Fe
Fe
O
C
Ta
Ta
Fe
Fe
Ta
Ta
Ta
Ta
Ta
2.00
4.00
6.00
8.00
10.00
12
keV